



DISCLAIMER

This report has been prepared by the Institute of Geological and Nuclear Sciences Limited (GNS Science) exclusively for and under contract to the Earthquake Commission. Unless otherwise agreed in writing by GNS Science, GNS Science accepts no responsibility for any use of, or reliance on any contents of this Report by any person other than the Earthquake Commission and shall not be liable to any person other than the Earthquake Commission, on any ground, for any loss, damage or expense arising from such use or reliance.

The data presented in this Report are available to GNS Science for other use from 1 January 2010

BIBLIOGRAPHIC REFERENCE

Robinson, R.; Rhoades, D.A.; Gerstenberger, M.C. 2009. Understanding a promising earthquake forecasting tool by computer modelling of seismicity, *GNS Science Consultancy Report CR 2009/342*

CONTENTS

TECHNICAL SUMMARY	III
NON-TECHNICAL SUMMARY	IV
1.0 INTRODUCTION	5
2.0 EEPAS MODEL	5
3.0 SYNTHETIC SEISMICITY	8
4.0 METHOD	10
5.0 FORECASTING RESULTS FOR THE NETWORK A CATALOGUE	16
6.0 FORECASTING RESULTS FOR THE NETWORK B CATALOGUE	17
7.0 CONCLUSION	22
8.0 ACKNOWLEDGEMENTS	22
9.0 REFERENCES	22

FIGURES

Figure 1	Examples of the precursory scale increase phenomenon in actual catalogues for major earthquakes at Loma Prieta (California), Kobe (Japan), Kithira (Greece), and Inangahua (New Zealand). (a) Epicentres of precursory earthquakes, mainshock and aftershocks. Dashed lines enclose the precursory area A_P . (b) Magnitudes versus time of prior and precursory earthquakes, also mainshock and aftershocks. Dashed lines show precursory increase in magnitude level. M_m is mainshock magnitude; M_P is precursor magnitude. (c) Cumag versus time (See equation 1). Dashed lines show precursory increase in seismicity rate. Protractor translates cumag slope into seismicity rate in magnitude units per year (M.U./yr), for times before the mainshock. Cumag values at the right hand ordinate refer to times beginning with the mainshock.	6
Figure 2	Precursory scale increase predictive relations between (a) mainshock magnitude M_m and precursor magnitude M_P ; (b) precursor time T_P and M_P ; (c) precursor area A_P and M_P . Dotted lines indicate 95% tolerance limits.	7
Figure 3	Surface traces of the 257 vertical, strike-slip faults in Network A.	12
Figure 4	Surface traces of the 55 major faults in the Wellington region model (Network B). Most faults are non-vertical and where they intersect at depth the one with lesser slip rate is truncated. The Wellington Fault is shown in red.	13
Figure 5	3000 small faults placed at random in Network B. Yellow are above the plate interface; green are below. The red rectangles are the surface projections of the parts of the plate interface on which seismic slip is likely although this is suppressed in the present study.	14
Figure 6	Spatial distribution of earthquake epicentres in (a subset of) the synthetic catalogue from network B.	15
Figure 7	Earthquake frequency - magnitude relation in (a subset of) the synthetic earthquake catalogue from network B.	16
Figure 8	Examples of the precursory scale increase phenomenon in the synthetic earthquake catalogue derived from network B. The major earthquakes represented here are the only ones that have been examined for the Ψ -phenomenon. For details of the plots, see the caption to Figure 1.	19
Figure 9	Precursory scale increase scaling relations between mainshock magnitude M_m and (a) precursor magnitude M_P ; (b) precursor time T_P ; (c) precursor area A_P (d) the product $A_P T_P$. Dotted lines indicate 95% tolerance limits calculated from real-world catalogues. Open symbols are used for data from real catalogues (Evison and Rhoades, 2004), and solid dots for those from synthetic catalogue derived from network B.	20
Figure 10	Shear stress (MPa, black) and strength (MPa, red) of one particular cell on the Wellington Fault through several seismic cycles. The cell is near all the hypocentres of the large events shown and is the initiation point for the last large event.	21

TABLES

Table 1	Information rate per earthquake I_M of the SUP, PPE and EEPAS models fitted to synthetic seismicity catalogues compared with corresponding statistics (Rhoades, 2009) from the ANSS catalogue of California and the NIED catalogue of the Kanto region, central Japan.	17
Table 2	EEPAS model parameters as fitted to the synthetic catalogue from network B, the ANSS catalogue of California and the NIED catalogue of the Kanto region, central Japan (Rhoades 2009, tables 1 - 3)	18
Table 3	Information rate per earthquake I_M^* of the SUP, PPE and EEPAS models tested on an independent subset of the synthetic seismicity catalogue from network B, compared with corresponding statistics (Rhoades, 2009) from the ANSS catalogue of California and the NIED catalogue of the Kanto region, central Japan.	19

TECHNICAL SUMMARY

The Every Earthquake a Precursor According to Scale (EEPAS) model has performed well as a long-range forecasting model for the larger earthquakes in a number of real seismicity catalogues. It is based on the precursory scale increase phenomenon and associated predictive scaling relations, the detailed physical basis of which is not well understood. Synthetic earthquake catalogues generated deterministically from known fault physics and long- and short-range stress interactions on fault networks have been analysed using the EEPAS model, to better understand the physical process responsible for the precursory scale increase phenomenon. In a generic fault network with a small number of parallel faults, the performance of the EEPAS model is poor. But in a more elaborate network involving major faults at a variety of orientations and a large number of small, randomly oriented faults, the performance of the EEPAS model is similar to that in real catalogues, such as that of California and central Japan, albeit with some differences in the scaling parameters for precursor time and area. The richness and variety of fault orientations therefore appear to be responsible for conformity to the EEPAS model. Tracking the stress evolution on a set of individual cells in the synthetic seismicity model may give insights into the origin of the precursory scale increase phenomenon. It is possible that introducing visco-elastic relaxation into the synthetic seismicity program could explain some of the differences in scaling parameters.

NON-TECHNICAL SUMMARY

A regular feature of many real earthquake catalogues is that major earthquakes are preceded in the long term by an increase in the rate and magnitude of minor earthquakes. The largest minor earthquakes involved in this increase are usually about one unit of magnitude smaller than the major earthquake itself. Moreover, the precursor time (the time between the onset of the increase and the occurrence of the major event) and the precursory area (the area in which the increase, the major event and its aftershocks all occur) both grow in a regular statistical way with earthquake magnitude. This phenomenon is known as the precursory scale increase. It has been used to construct an earthquake forecasting tool, which works quite well in a number of earthquake prone regions, including New Zealand, California, Japan and Greece.

Why the precursory scale increase occurs is not well understood. In this study we try to understand it better by the use of computer-generated earthquake catalogues derived using simple assumptions about the physics of earthquake occurrence and the distribution of earthquake faults in the ground. If a computer-generated catalogue displays the precursory scale increase phenomenon, then perhaps the assumptions on which it is based are responsible for the phenomenon occurring in real catalogues.

It turns out that the distribution of faults in the ground is the key to the occurrence of the precursory scale increase phenomenon in the computer-generated catalogues. In a simple fault network with a small number of parallel faults, the precursory scale increase hardly occurs at all and the forecasting tool performs poorly. But in a more elaborate network involving major faults at a variety of orientations and a large number of small, randomly oriented faults, the precursory scale increase occurs before most major earthquakes and the forecasting tool performs well. Moreover the relations connecting earthquake magnitude, precursor time and precursory area are broadly similar.

The richness and variety of fault orientations therefore appear to be responsible for the precursory scale increase phenomenon. And the occurrence of the precursory scale increase in a computer-generated catalogue lends increased credence both to the forecasting tool and to the physical assumptions incorporated in the computer model. However there are some differences in detail between the patterns seen in the real and computer-generated catalogues. These could be investigated by further work on the computer model. This might include tracking changes of stress leading up to an earthquake on a major fault, and introducing more details of the physics of earthquake occurrence into the model.

1.0 INTRODUCTION

The aim of this project was to begin a study of the effectiveness of the Every Earthquake a Precursor According to Scale (Rhoades and Evison, 2004; EEPAS from here on) earthquake forecasting tool in forecasting the major earthquakes in synthetic catalogues generated by a physically realistic computer simulation of seismogenesis (Robinson, 2004). The EEPAS method has been derived and tested using several real-world earthquake catalogues, e.g. from New Zealand and California (Rhoades and Evison, 2004; Rhoades, 2007), Japan (Rhoades and Evison, 2005; 2006), and Greece (Console et al., 2006). In these tests the method has proved superior to several other forecasting models. Still, the real world catalogues have shortcomings that leave room for improvements: they are generally short (a few decades), incomplete (missing events), and inhomogeneous due to changes in processing methods. Synthetic seismicity catalogues can potentially overcome these shortcomings at the expense of some simplifications in the physics. Thus the results of this study, if positive, would serve to bolster both modelling aspects – EEPAS and synthetic seismicity. If unsuccessful or only partially successful, the results could lead to an understanding of how to improve both aspects. Because of the limited resources available for this study, the results presented here are only preliminary.

Below we give brief outlines of both the EEPAS forecasting model and the synthetic seismicity computer model. We then describe how we use the synthetic catalogues to test the EEPAS method (and vice versa). The results and their implications are discussed and suggestions for future work presented. This work has been presented at the SCEC annual meeting, 2009.

2.0 EEPAS MODEL

In the seismicity of well-catalogued regions from a variety of tectonic settings, major shallow earthquakes are usually preceded in the long term by an increase in both the magnitude level and the rate of occurrence of minor earthquakes, in a region not much larger than that later occupied by the epicentres of the major earthquake and its aftershocks. This is known as the precursory scale increase (or Ψ -) phenomenon (Evison & Rhoades, 2002, 2004). The precursory swarm (Evison, 1977) is a special case that occurs commonly in subduction regions and other areas of high fluid pressure.

The increase in rate of occurrence is calculated by means of the cumulative magnitude anomaly (cumag), $C(t)$, which is defined by

$$C(t) = \sum_{t_s \leq t_i \leq t} (M_i - M_c + 0.1) - k(t - t_s) \quad (1)$$

where

$$k = \sum_{t_s \leq t_i \leq t_f} (M_i - M_c + 0.1) / (t_f - t_s). \quad (2)$$

Here, M_i is the magnitude and t_i the time of the i th earthquake in the region, M_c is the threshold magnitude, and k is the average rate of magnitude accumulation between the starting time t_s and the finishing time t_f .

Examples of the Ψ -phenomenon are shown in Figure 1, for the M7.0 Loma Prieta, California, earthquake of 1989.10.18, the M7.2 Kobe, Japan, earthquake of 1995.01.17, the M6.4 Kithira, Greece, earthquake of 1997.10.13, and the M6.7 Inangahua, New Zealand, earthquake of 1968.05.23. In each example: plot (a) shows the area in which the phenomenon was observed, together with the epicentres of the precursory earthquakes, mainshock and aftershocks; plot (b) is a magnitude versus time plot for earthquakes inside the region; and plot (c) is a cumag plot finishing at the time of the mainshock. A second cumag covers the period from the occurrence of the mainshock to the end of the aftershocks. The onset of Ψ is marked by the minimum of the cumag. The slopes of dotted lines in Figure 1(c) represent the average rates of magnitude accumulation in magnitude units per year (M.U./yr), as indicated by the protractor, in the prior and precursory time periods, i.e. before and after the onset. The ratio of the latter rate to the former is the rate increase. A value of about 10 is typical. For each instance of Ψ the area is chosen to maximise the rate increase, and the starting-time is chosen so that the prior and precursory time periods are of similar lengths. The dotted lines in the (b) plots show a jump in the magnitude level at the time of the onset from the prior level to the precursory level M_P , where these levels are the average of the three largest earthquakes in the respective time periods.

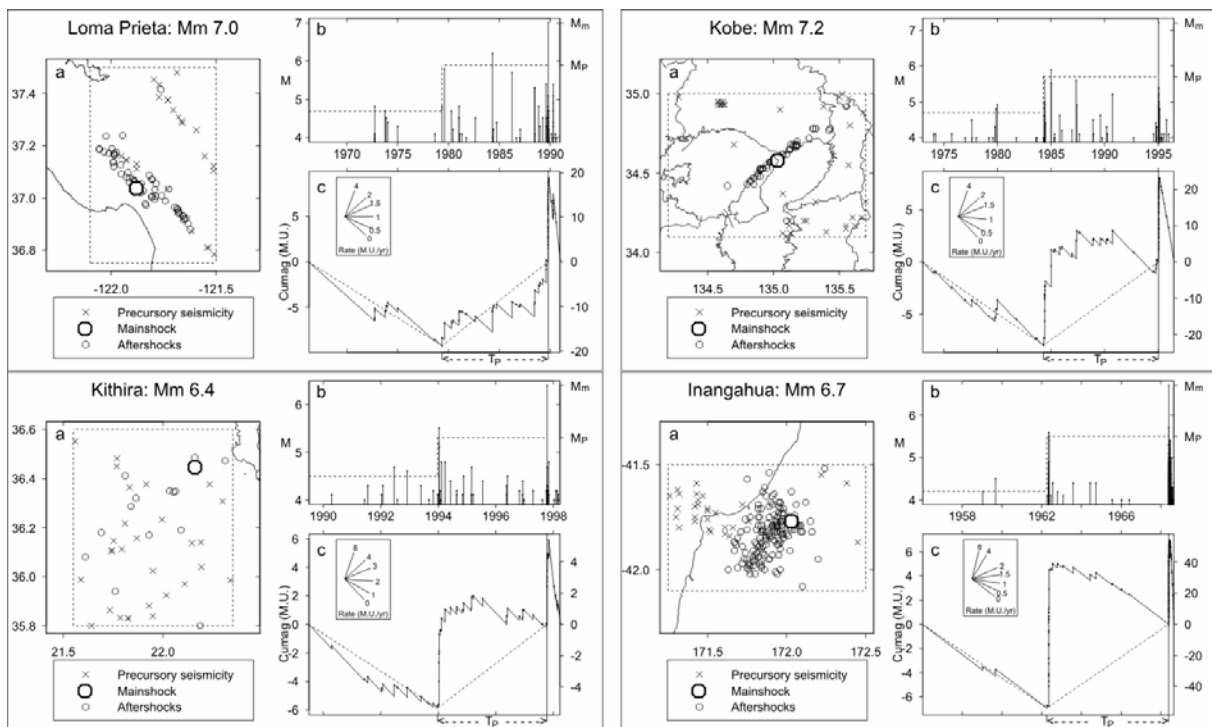


Figure 1 Examples of the precursory scale increase phenomenon in actual catalogues for major earthquakes at Loma Prieta (California), Kobe (Japan), Kithira (Greece), and Inangahua (New Zealand). (a) Epicentres of precursory earthquakes, mainshock and aftershocks. Dashed lines enclose the precursory area A_P . (b) Magnitudes versus time of prior and precursory earthquakes, also mainshock and aftershocks. Dashed lines show precursory increase in magnitude level. M_m is mainshock magnitude; M_P is precursor magnitude. (c) Cumag versus time (See equation 1). Dashed lines show precursory increase in seismicity rate. Protractor translates cumag slope into seismicity rate in magnitude units per year (M.U./yr), for times before the mainshock. Cumag values at the right hand ordinate refer to times beginning with the mainshock.

The key variables to be noted from any instance of the Ψ -phenomenon are the mainshock magnitude, M_m , the precursor magnitude, M_P , the precursor time T_P (the time between the onset of Ψ and the mainshock) and the size A_P of the area in which the phenomenon is

observed. Analysis of 47 instances of Ψ showed that all of these variables are linked by simple scaling relations, and hence M_P is predictive of the time, magnitude and location of the major earthquake (Evison & Rhoades, 2004). The predictive scaling relations are shown in Figure 2. They consist of linear regressions of M_m , $\log T_P$ and $\log A_P$ on M_P .

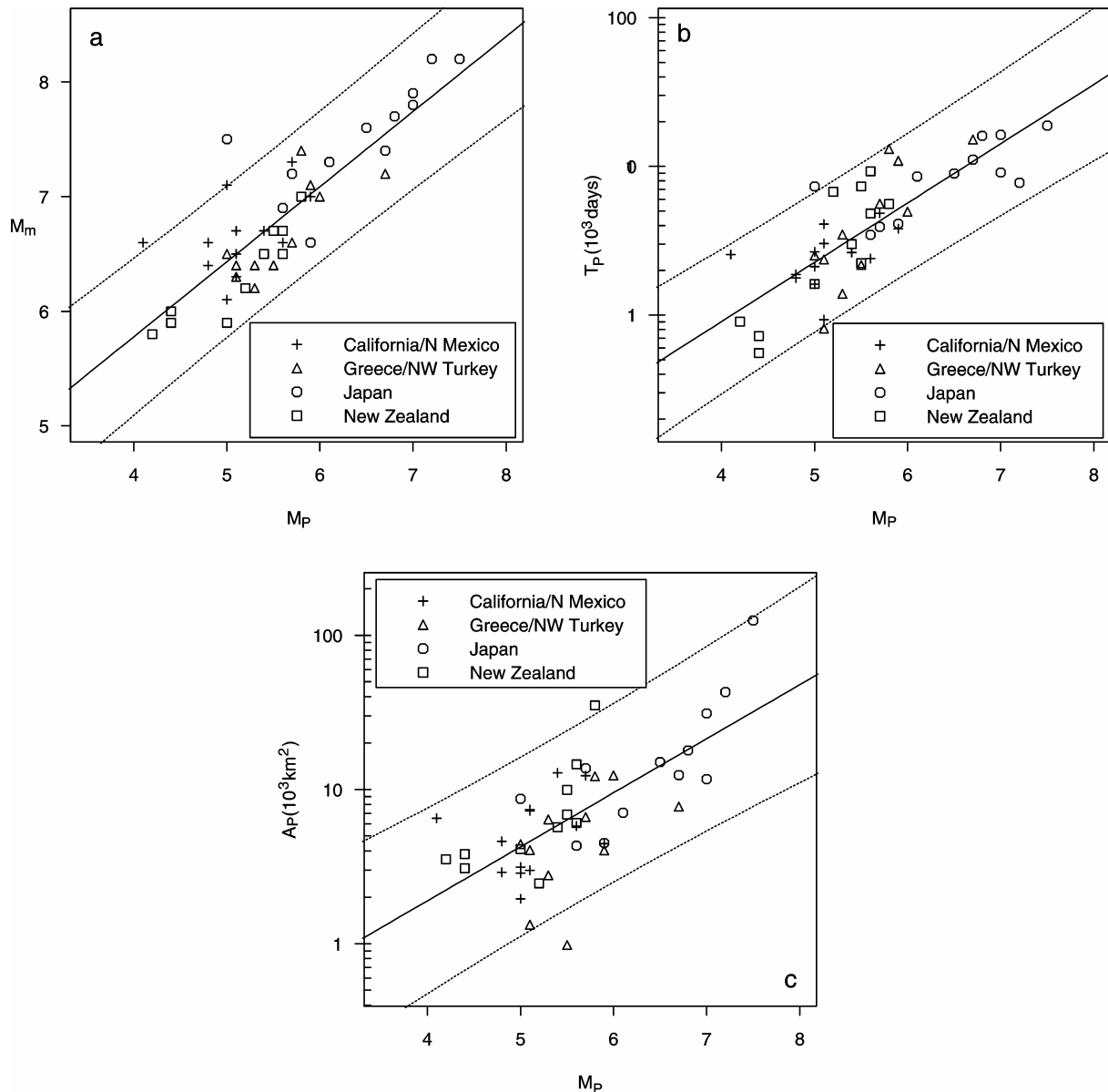


Figure 2 Precursory scale increase predictive relations between (a) mainshock magnitude M_m and precursor magnitude M_P ; (b) precursor time T_P and M_P ; (c) precursor area A_P and M_P . Dotted lines indicate 95% tolerance limits.

The EEPAS forecasting model is a space-time point-process model which adopts the Ψ predictive scaling relations (Fig. 2), and applies them to all earthquakes, regarding each earthquake as a long-term precursor of larger earthquakes to follow later. In this model, the rate density of future earthquake occurrence at any given time, magnitude and location is derived directly from the times of occurrence, magnitudes and locations of past earthquakes in the catalogue, with every earthquake making a transient contribution. The magnitude of each earthquake determines, through the scaling relations, its contribution to the future rate density of earthquake occurrence. A weighting strategy that takes account of neighbouring earthquakes may be applied, so that aftershocks make only a small contribution. For the

parameterisation and other details, see Rhoades & Evison (2004). Briefly, the main parameters of the EEPAS model are closely linked to the predictive scaling relations (Figure 2): a_M, b_M and σ_M to the intercept, slope and standard deviation, respectively, of the regression of mainshock magnitude on precursor magnitude; a_T, b_T and σ_T to the intercept, slope and standard deviation, respectively, of the regression of the logarithm of precursor time on precursor magnitude; and b_A and σ_A to the slope and intercept, respectively, of the regression of the logarithm of precursor area on precursor magnitude.

The EEPAS model has been successfully applied to several regional earthquake catalogues, including those of New Zealand, California, Japan, Greece, and the Kanto region of central Japan (Rhoades and Evison, 2004, 2005, 2006; Console et al., 2006; Rhoades, 2007). In fitting and in independent testing, it generally explains the occurrence of the major earthquakes much better than either a stationary uniform Poisson (SUP) baseline model or a quasi-static baseline model with a location distribution based on proximity to the epicentres of past earthquakes (PPE), which was adapted by Rhoades and Evison (2004) from a model proposed by Jackson & Kagan (1999). EEPAS has also been combined in a mixture with a short-term earthquake probability model (STEP) incorporating Omori-Utsu law decay of aftershocks to give improved forecasting performance (Rhoades and Gerstenberger, 2009), and an elaboration of the model which allows for aftershocks of predicted mainshocks has been described (Rhoades, 2009), again leading to improved forecasting performance.

The EEPAS model is itself a mixture of two components: a time varying component based on the Ψ -phenomenon, as described above, and the quasi-static PPE model, also described above. The mixing parameter μ , which has possible values between 0 and 1, controls the weight to be given to the PPE model in this mixture. A value of $\mu = 0$ implies that nearly all earthquakes in the target set display the precursory scale increase phenomenon and are predictable to some degree. A value of $\mu = 1$ implies that no earthquakes in the target set display the precursory scale increase, and that earthquakes occur close to where they have in the past, but with no predictability of their times of occurrence. In previous studies on actual catalogues, the optimal value of μ has ranged between 0 and 0.3. There is a tendency for μ to decrease as the magnitude threshold of the target earthquakes is increased.

3.0 SYNTHETIC SEISMICITY

In recent years the field of study termed “synthetic seismicity” has developed in order to help address problems due to deficiencies in real-world catalogues (Dieterich, 1994; Ben-Zion, 1996; Robinson & Benites, 1996; Ward, 2000; Fitzenz & Miller, 2001; Rundle et al., 2006; Robinson, 2004; Robinson et al, 2009). By synthetic seismicity we mean a computer model of a fault network that generates catalogues of earthquakes based on our knowledge of the physics of seismogenesis and fault interaction. Such catalogues are, by definition, homogeneous (e.g., magnitudes are calculated uniformly through time), can be as long as our patience and computer resources allow, and are complete to the degree that all the known major faults are included along with many more smaller ones. In cases where the application is meant to mimic a specific real region, the model is “tuned” to reproduce the observed statistics of the actual seismicity of the region (e.g., b-value, rates of activity, moment-area scaling) and geologic estimates of the long-term slip rates on major faults. This tuning involves both the adjustment of individual fault loading rates and fault mechanical parameters such as stress-drop and coefficients of friction. Generally the catalogues are made long enough to yield statistically reliable information and to sample the complete range

of interactions amongst events. Of course, the model's answers to our questions are believable only if the synthetic model captures real-world fault behaviour to an acceptable degree. The synthetic seismicity model used in this study is very similar to that described fully by Robinson & Benites (1996, 2001), Robinson (2004) and Robinson et al. (2009). The model differs from most others in that faults of any orientation and sense of slip are embedded in a fully 3D elastic half-space, fault rupture is pseudo-dynamic, the cell size (each fault is sub-divided into smaller cells) can be small enough that rupture histories can be used to generate strong-motion seismograms, and induced changes in pore pressure are included. Except for the pore pressure aspects, the model as used here is entirely elastic.

The model consists of five key elements: 1) A geometric description of the faults, which are finely divided into smaller cells; 2) frictional behaviour defined by a variable coefficient of friction and of static/dynamic type, with healing; 3) a driving mechanism that loads the faults toward failure; 4) fault failure based on the Coulomb Failure Criterion; and 5) fault interactions via induced changes in static stress and pore pressure. The driving mechanism results in the initial failure of one fault cell that in turn induces changes in stress and pore pressure on all other cells, on all faults, after allowing for stress propagation time. If loaded sufficiently, other cells then fail as part of the same event, and so on. The more cells that slip during a failure episode the bigger is the synthetic earthquake. Thus, once the initial conditions of the model have been specified, the model is deterministic, not stochastic. The formulation of Okada (1992) for a uniform elastic half-space is used to calculate the induced displacements and their spatial derivatives, and hence strains and stresses. Induced stresses propagate through the medium at the shear-wave velocity. In this study the model rigidity is $4.0 \times 10^{10} \text{ Nm}^{-2}$ and the density is $2.65 \times 10^3 \text{ kgm}^{-3}$. These average values are considered to be reasonable first approximations for the brittle crust in New Zealand. The coefficients of friction (dry, and variable from cell to cell) range from 0.7 to 0.8, consistent with both laboratory and field evidence (Byerlee, 1978; Raleigh et al., 1976). We do not use the more common "apparent coefficient of friction" that only approximates the effect of pore pressure. Instead we prefer the more realistic treatment in which pore pressure changes can be positive or negative, in proportion to the induced dilation or compaction (Beeler et al., 2000) and decay with time. This does involve the assumption of a constant Skempton's coefficient, here taken as 0.5. The stress drop on a cell that fails is uniformly 30%, and healing occurs after 3.0 seconds (Heaton, 1990).

An important additional factor in our model is what we call the "dynamic enhancement factor, DEF). This factor gives the amplification of the induced stresses near the edges of a propagating rupture front. It is applied only for one (very short) time step and only for the immediate neighbours of a rupturing cell (Robinson & Benites, 2001). The DEF is meant to mimic the stress enhancements found in more detailed models of crack propagation that would require far too much computation in our case. It has two primary effects: 1) ruptures tend to cascade more easily; and 2) ruptures can sometimes jump across from one fault segment to another offset segment if the two segments are not too far apart. The value used here, 3.0, was not picked arbitrarily, but is the value that was found necessary in our previous work to match detailed computational studies of en echelon faults (Harris & Day, 1999) and to match the probability of jumps as observed in the real world, i.e. about 50% for a separation of 1 km. (Wesnousky, 2008).

Because the synthetic seismicity model is computationally intense, the success of a project depends on calculating all cell interaction terms at the start and storing them in memory. This in turn places a limit on the extent of the fault network and the cell size. Another aspect that

decreases computation is that there are two sizes of time step. The first is quite short (0.2 to 0.8 sec here, based on cell size and stress propagation velocity) and is used during the rupture process and the second is variable and much longer, corresponding to the time needed for the next rupture episode to start (this can be calculated from the loading rates and current stresses). For this project, most computations have been done on GNS Science's parallel processing computers.

It should be noted that the synthetic seismicity model is not a continuum model; stress is monitored only on the fault cells and not everywhere as might be the case in a finite-element model. Still, the large number of small faults included in most of our models serves in some degree to make it similar to a continuum model.

Our synthetic seismicity model, sometimes known as ARTS (ARTificial Seismicity), was first applied to a study of the Wellington region in 1996 (Robinson & Benites, 1996). That was a study that involved only the 6 most major faults and was designed to answer EQC's concern about multiple large events within a short time span. The answer was that close temporal clustering of large events was likely. Since then the model, or its extensions (Robinson, & Benites, 2001), have been used to study the Marlborough fault network (Robinson, 2004) and the Taupo rift (Robinson et al., 2009). The model has also been presented to a SCEC (Southern California Earthquake Center) workshop. Another study focused on the Wellington Fault in isolation (as a single planar segment) for producing detailed time histories of a characteristic rupture and the calculation of the corresponding strong ground motion (Benites et al., 2003).

In addition to these previous studies of specific real-world fault networks, we have also used the synthetic seismicity method to investigate the Accelerating Moment Release forecasting method (AMR; Robinson et al, 2005; Zhou et al, 2006). In the AMR method it is proposed that there is a build up in moment (M_0) release in a wide area surrounding a forthcoming large quake. The specific form of that build up in general is a power law of time-cumulative $M_0^{0.5}$. When a critical point is reached, the large event occurs. However, our results were mostly negative, i.e. there was no universal AMR pattern before the largest events. The synthetic catalogue used by Robinson et al. (2005) was a generic strike-slip network, the same one used here for Model A. Zhou et al. (2006) used a very simple model of the Wellington region.

4.0 METHOD

The basic method used here is to derive EEPAS coefficients for two synthetic catalogues and to compare the fit and performance of EEPAS with that of two other forecasting methods, namely the SUP and PPE models described above. In the EEPAS model, all earthquakes are weighted equally, because the synthetic catalogues do not include strongly clustered aftershock sequences. The SUP model is a model of "least information" in that it contains no spatial or time-varying information on earthquake occurrence, although it does incorporate the total number of earthquakes above the target magnitude threshold in the region of study, and the magnitude distribution as summarised by the b-value of the Gutenberg-Richter frequency-magnitude law. As well as incorporating these elements, the PPE model also contains information on the smoothed spatial distribution of past earthquakes in the catalogue. It does not include any explicit time-varying estimate component, but its estimate of the spatial distribution of earthquake occurrence varies slowly

with time as new earthquakes are added to the catalogue. Thus the PPE model is expected to provide the best fit and performance if the time variation of seismicity does not conform to the EEPAS model, i.e., if the precursory scale increase does not occur before major earthquakes in the synthetic catalogues.

It is convenient to assess the goodness of fit of a model using the Akaike Information Criterion (AIC) statistic (Akaike, 1974), defined for a particular model M as

$$AIC_M = -2 \ln L_M + 2p_M \quad , \quad (3)$$

where $\ln L_M$ is the optimised log likelihood of the model, and p_M is the number of fitted parameters. A relatively low value of AIC indicates a relatively high information value, i.e., a model which explains the data relatively well. Formally the information value of a fitted model can be expressed as the information rate per earthquake, I_M , defined by

$$I_M = (AIC_{SUP} - AIC_M) / (2N) \quad (4)$$

where N is the number of earthquakes in the target set and AIC_{SUP} is the AIC value for the SUP model. Thus I_{SUP} is 0 by definition. For the measurement of performance on independent data, the information rate per earthquake I_M^* for a model M is defined as

$$I_M^* = (\ln L_M - \ln L_{SUP}) / N \quad (5)$$

where $\ln L$ is the log likelihood statistic and N is the number of target earthquakes in the testing set. We note that I_M and I_M^* differ only in the absence of a correction for the number of parameters in I_M^* . The number of fitted parameters does not affect the information score for independent testing because the parameter values are all fixed at the testing stage.

We have tested the EEPAS forecasting method using synthetic seismicity catalogues derived from two fault networks. The first, Network A (Figure 3), is a generic strike-slip fault network (i.e. not based on a specific real-world network) consisting of 256, parallel, strike-slip faults embedded in a region 500 km by 500 km, and 20 km in depth. The faults all have the same strike and are all vertical. There is one major fault at the centre ($L = 75$ km, $W = 20$ km), and the size distribution of the others is taken to give a b-value of ~ 1.0 . Characteristic events on the major fault have magnitudes of 7.1 - 8.1 and an average recurrence time of 160 years. This is the same network used by Robinson et al (2005), who failed to find much evidence for the AMR forecasting method. For this study we have used characteristic events on the central fault as the "target" events.

Network A: 257 vertical strike-slip faults, maximum magnitude 7.3

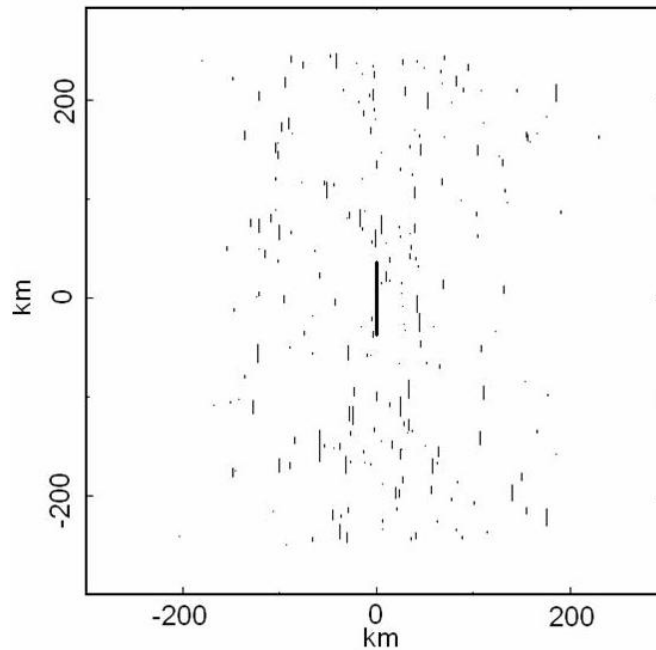


Figure 3 Surface traces of the 257 vertical, strike-slip faults in Network A.

The second network (Network B) is similar to the Wellington region fault network used in the EQC funded “Its Our Fault” (IOF) project. The synthetic seismicity aspects of IOF are described in detail in Robinson et al. (2009). The fault network consists of 55 major faults, subdivided into from 1 to 5 segments (Figure 4). Strikes, dips, and rakes are quite variable. Although the majority of the faults are primarily strike-slip, there are also thrust and normal types. Even the strike-slip faults are rarely vertical: the Wellington Fault, for example, consists of 5 segments with dips from 65° to 90° and strikes from 40° to 66° . For this study we have suppressed large subduction interface events because it is unclear what proportion of slip on the interface occurs as aseismic slip. In addition to the major faults, the network contains 3000 small faults (Figure 5) placed in the model in a way that mimics the distribution of present day background seismicity. Epicentres for a subset of the catalogue are shown in Figure 6. The regional b-value is near 1.0 with a “characteristic hump” at the large magnitude end (Figure 7). For this study we have selected 43 large events on the Wellington area fault network as the “target” events for the fitting of seismicity models. Although network B is based on a model of the Wellington region, how well it represents the actual fault network of the Wellington region is of no consequence in this study.

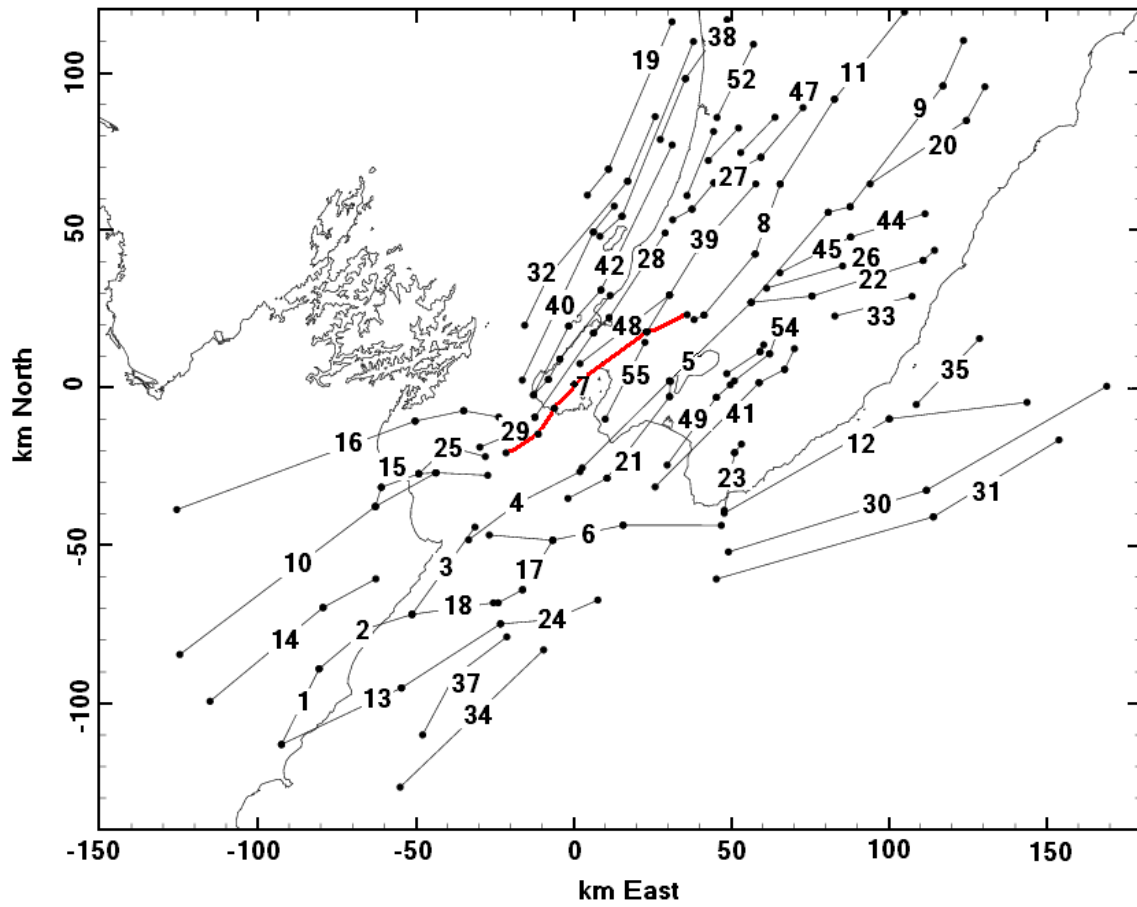


Figure 4 Surface traces of the 55 major faults in the Wellington region model (Network B). Most faults are non-vertical and where they intersect at depth the one with lesser slip rate is truncated. The Wellington Fault is shown in red.

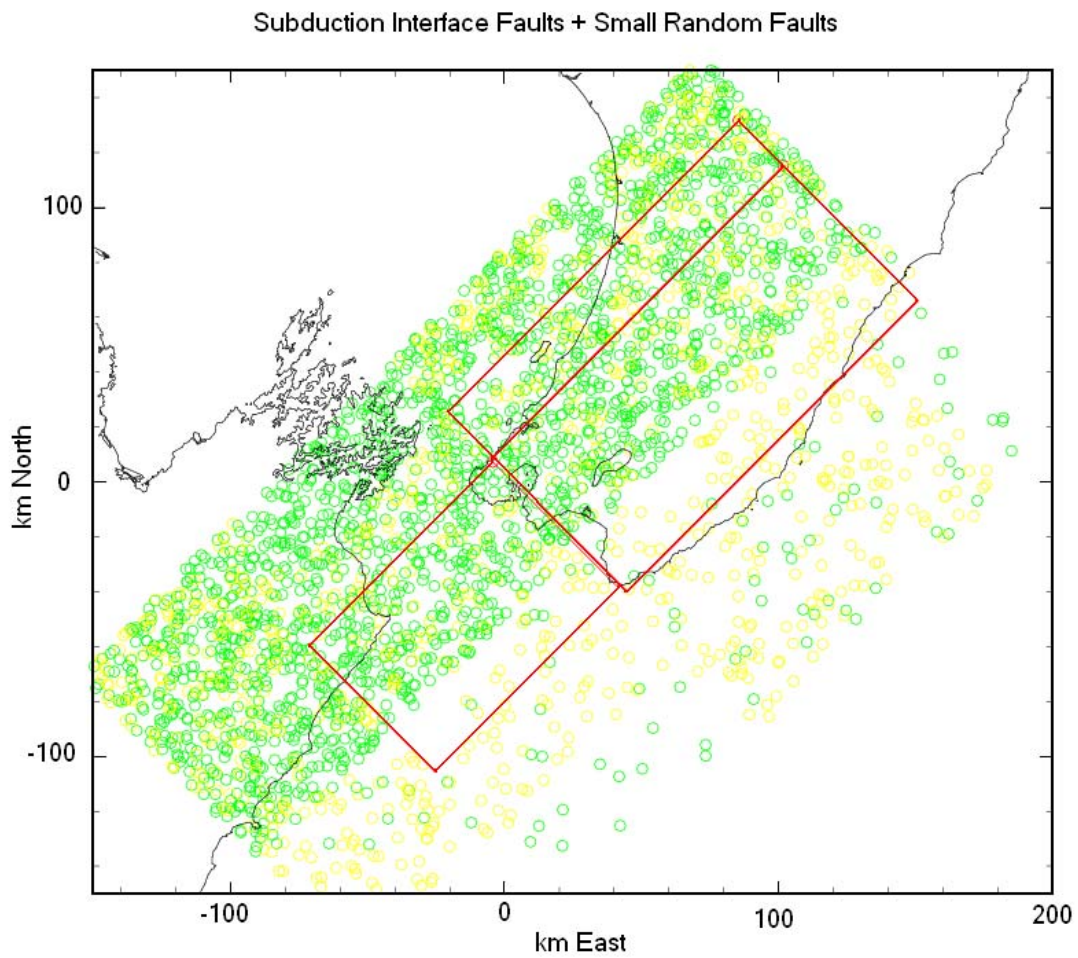


Figure 5 3000 small faults placed at random in Network B. Yellow are above the plate interface; green are below. The red rectangles are the surface projections of the parts of the plate interface on which seismic slip is likely although this is suppressed in the present study.

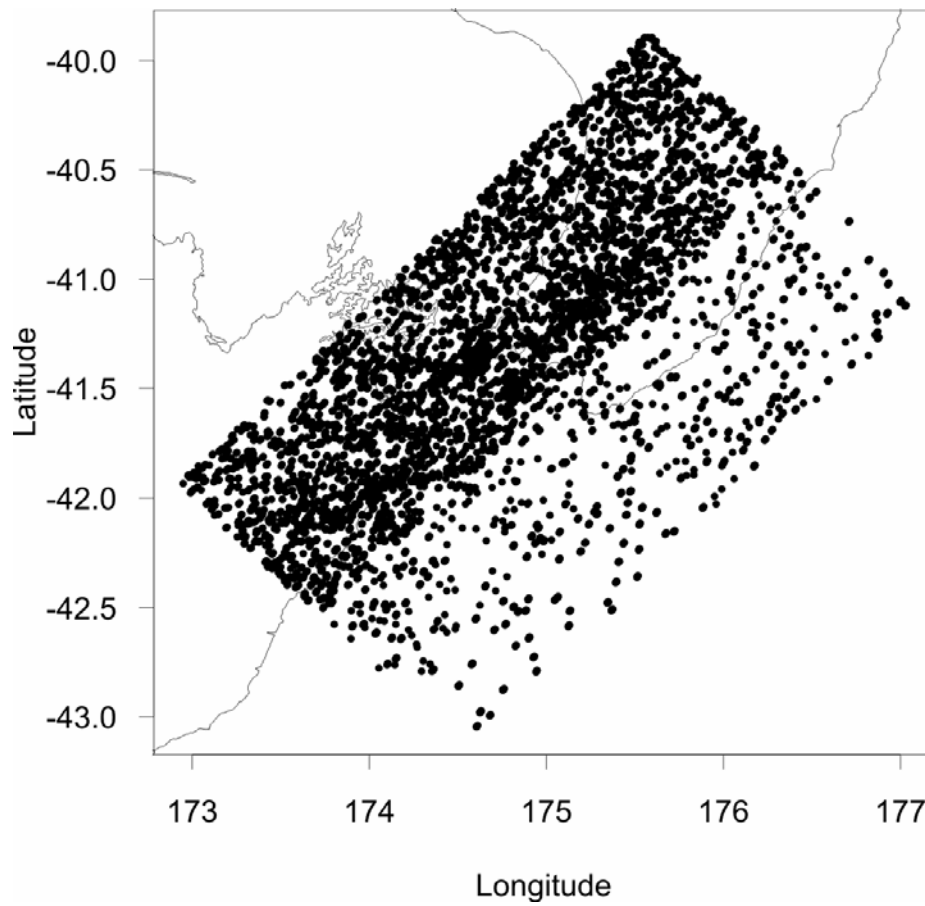


Figure 6 Spatial distribution of earthquake epicentres in (a subset of) the synthetic catalogue from network B.

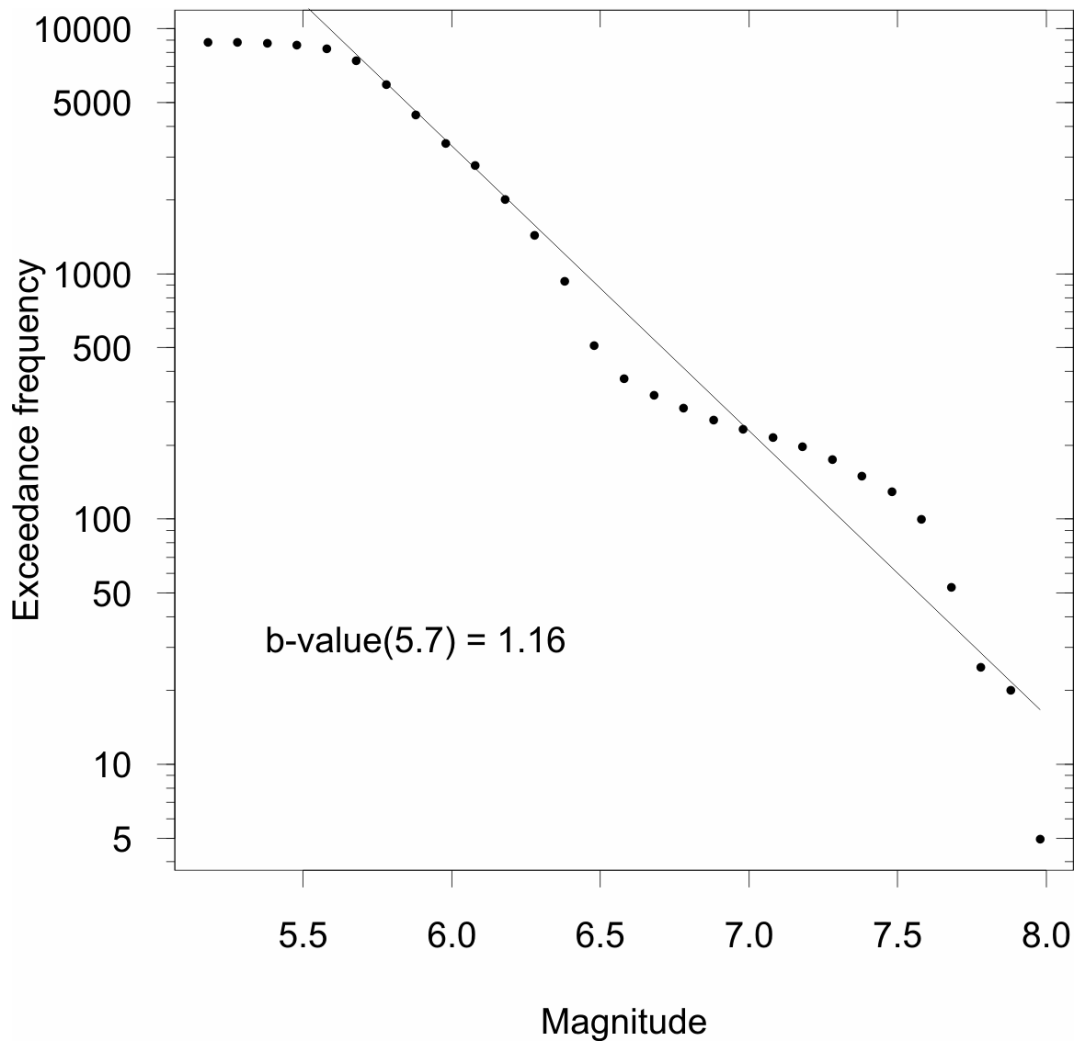


Figure 7 Earthquake frequency - magnitude relation in (a subset of) the synthetic earthquake catalogue from network B.

5.0 FORECASTING RESULTS FOR THE NETWORK A CATALOGUE

The EEPAS, PPE and SUP models were optimised for a 2600 year subset of the synthetic catalogue from Network A using the magnitude thresholds $m_0 = 4.85$ (the smallest magnitude included in the catalogue), and $m_u = 8.15$ (the largest magnitude for any earthquake in the catalogue and the upper magnitude limit of the target set). Various values of the lower magnitude threshold m_c for the target set were used, namely, 6.85, 6.95 and 7.35, giving $N = 617$, 531 and 150 earthquakes in the target set, respectively. Four EEPAS parameters were fitted – a_M , a_T , σ_A and μ , with other parameters being set to values from previous studies. For comparison, the PPE model has three fitted parameters and the SUP model one fitted parameter. The same Gutenberg-Richter b-value was used for all three models.

In all cases, the best fitting model was PPE. The EEPAS model, when optimised with an upper limit for μ of less than one, attained a maximum likelihood value less than that of the PPE model. For example, with a $m_c = 7.35$ and an upper limit for μ of 0.4, the information rate per earthquake I_{EEPAS} was 1.15 (see Table 1) compared to $I_{PPE} = 1.36$. In all three cases, when optimised with an upper limit of 1 for μ , the EEPAS model attained a maximum likelihood equal to that of the PPE model, with the optimum value μ being 1.

Table 1 Information rate per earthquake I_M of the SUP, PPE and EEPAS models fitted to synthetic seismicity catalogues compared with corresponding statistics (Rhoades, 2009) from the ANSS catalogue of California and the NIED catalogue of the Kanto region, central Japan.

Model	Information rate per earthquake I_M			
	Network A	Network B	California	Kanto
SUP	0.0	0.0	0.0	0.0
PPE	1.36	0.81	1.65	1.47
EEPAS	1.15	1.35	1.97	1.89

It is clear from this result that the earthquakes in the synthetic catalogue derived from Network A do not display the precursory scale increase phenomenon to any significant degree. This result is in strong contrast to previous results for the EEPAS model on real-world catalogues of New Zealand, California, Japan and Greece, in which the EEPAS model has consistently been found to fit better than the PPE model with an optimal value of μ in the range 0 – 0.3.

6.0 FORECASTING RESULTS FOR THE NETWORK B CATALOGUE

The EEPAS, PPE and SUP models were optimised for a 5000 year period of the synthetic catalogue from Network B using the magnitude thresholds $m_0 = 5.65$, $m_c = 7.65$, and $m_u = 8.55$. This gave 43 earthquakes in the target set. As in the case of the network A catalogue, four EEPAS parameters were fitted – a_M , a_T , σ_A and μ , with other parameters being set to values from previous studies.

In this case the EEPAS model gave the best fit to the data. The information rates per earthquake were $I_{EEPAS} = 1.35$ and $I_{PPE} = 0.81$ (Table 1). Table 1 shows comparable values from fitting the same parameters of the EEPAS model to real-world catalogues of California and the Kanto region in central Japan. Note that the value of I_{PPE} reflects the degree of spatial heterogeneity of seismicity in the target region, which is relatively low in the case of the synthetic network because the target region is filled with a rather dense network of faults (Figures 4 and 5), with the main inhomogeneity being a lower level of seismicity in the southeast part of the region compared to that in the northwest (Figure 6).

The difference in the information scores of the EEPAS and PPE models is an indication of the predictability of the times and locations of the target events as compared to the predictability of their locations alone. Here $I_{EEPAS} - I_{PPE}$ is 0.54 for the network B synthetic catalogue, compared to values of 0.34 and 0.42 for the California and Kanto catalogues, respectively. The large earthquakes in this synthetic catalogue are therefore at least as predictable as those in actual catalogues, although the magnitude range of the target set is narrower than for the real-world catalogues.

The optimal EEPAS model parameters are shown in Table 2, and again compared to optimal parameters from the California and Kanto regions. When other parameters are equal, as they are constrained to be here, the values of a_M , a_T and σ_A can be interpreted as indexes of the relation between precursory earthquakes and major earthquakes in magnitude, time and location, respectively. Specifically: a_M indicates the typical difference in magnitude between the mainshock and its most significant precursors; the precursor time is proportional to 10 to the power of a_T ; and the precursory area is proportional to σ_A^2 . The value of a_M in the

synthetic catalogue is similar to that of California and Kanto, indicating that the magnitude relation between precursors and major earthquakes is similar to that of real-world catalogues. The value of a_T is larger than in both California and Kanto, indicating precursor times which are longer by a factor of 2.8 than those in California and by a factor of 18 than those in Kanto. On the other hand, the value of σ_A is smaller than in both California and Kanto, indicating precursory areas which are smaller by a factor of 3.1 than those in California and by a factor of 21 than those in Kanto. Finally, we note that the value of μ in the synthetic catalogue (0.15) is similar to that of the California and Kanto catalogues, indicating that in all three catalogues a high proportion of major earthquakes exhibit the precursory scale increase phenomenon.

Table 2 EEPAS model parameters as fitted to the synthetic catalogue from network B, the ANSS catalogue of California and the NIED catalogue of the Kanto region, central Japan (Rhoades 2009, tables 1 - 3)

Parameter	Catalogue		
	Synthetic (network B)	California ($m_c = 4.95$)	Kanto ($m_c = 4.75$)
a_M	1.26	1.00	1.37
b_M	1.0*	1.0*	1.0*
σ_M	0.32*	0.32*	0.32*
a_T	2.56	2.11	1.31
b_T	0.40*	0.40*	0.40*
σ_T	0.23*	0.23*	0.23*
σ_A	0.48	0.84	2.19
b_A	0.35*	0.35*	0.35*
μ	0.15	0.20	0.14

* Fixed parameter

The performance of the EEPAS model, with the optimal parameters of Table 2, was applied to an independent period of 5000 years of the synthetic catalogue from network B. The target set contained 49 earthquakes with $M > 7.65$. The information scores I_M^* of the SUP, PPE and EEPAS models were compared with each other, and with the outcome of similar performance tests on the California and Kanto catalogues (Rhoades, 2009). The results are shown in Table 3. Again the difference in the information scores of the EEPAS and PPE models is an indication of the predictability of the times and locations of the target events as compared to the predictability of their locations alone. In this case, there is no bias due to fitting of parameters. We note that $I_{EEPAS}^* - I_{PPE}^*$ is 0.34 for the network B catalogue, compared to 0.71 for California and 0.23 for Kanto. This difference quantifies the amount of time-varying varying information (or predictability) in the EEPAS forecasts. Thus the major earthquakes in the synthetic catalogue for network B have a level of predictability which is comparable to those in actual catalogues.

Table 3 Information rate per earthquake I_M^* of the SUP, PPE and EEPAS models tested on an independent subset of the synthetic seismicity catalogue from network B, compared with corresponding statistics (Rhoades, 2009) from the ANSS catalogue of California and the NIED catalogue of the Kanto region, central Japan.

Model	Information rate per earthquake I_M^*		
	Network B	California	Kanto
SUP	0.0	0.0	0.0
PPE	0.89	1.01	1.27
EEPAS	1.13	1.72	1.50

A sample of 14 major earthquakes in the synthetic catalogue from network B was examined individually for evidence of the Ψ -phenomenon, using the graphical approach of Figure 1. In each case it was possible to identify a long-term precursory scale increase in the vicinity of the major event. Four examples are shown in Figure 8. These are in many respects similar to the real-world examples of Figure 1: the onset of Ψ occurs suddenly and involves an increase in both the rate and magnitude of earthquake occurrence, and the difference between M_m and M_p is about one magnitude unit. However, the difference between the precursory and prior magnitude levels is on average smaller than those in Figure 1 and in most other real-world examples: a difference of about 1 is typical (Evison and Rhoades 2004), but the average difference here is less than 0.5. This may be an effect related to the somewhat unusual magnitude distribution in this synthetic catalogue (Figure 7), which does not follow the Gutenberg-Richter law as closely as most real-world catalogues.

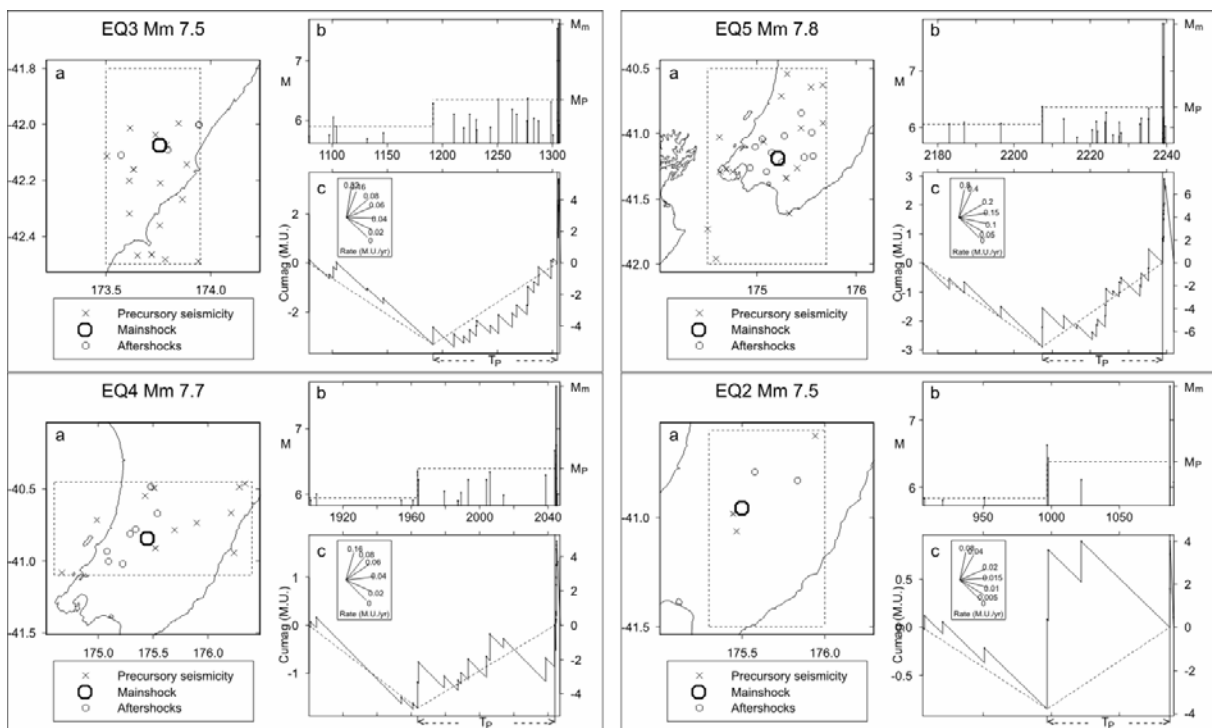


Figure 8 Examples of the precursory scale increase phenomenon in the synthetic earthquake catalogue derived from network B. The major earthquakes represented here are the only ones that have been examined for the Ψ -phenomenon. For details of the plots, see the caption to Figure 1.

The values of M_m , M_P , A_P and T_P from the 14 examples of Ψ in the synthetic catalogue have been added to previously published scaling relations (Evison and Rhoades, 2004) in Figure 9, in which they appear as solid dots. Each of the plots in this figure shows the relation between M_m and another variable. It can be seen that the synthetic data fit well to the published relation between M_P and M_m , but not so well to those between T_P and M_m and between A_P and M_m . The synthetic values of T_P tend to be high relative to the published relation, on average by a factor of 2.5. The values of A_P tend to be low compared to the published relation, on average by a factor of 2.7. Because of these counterbalancing effects, the synthetic values of the product $A_P T_P$ fit well to the published relation of $A_P T_P$ and M_m .

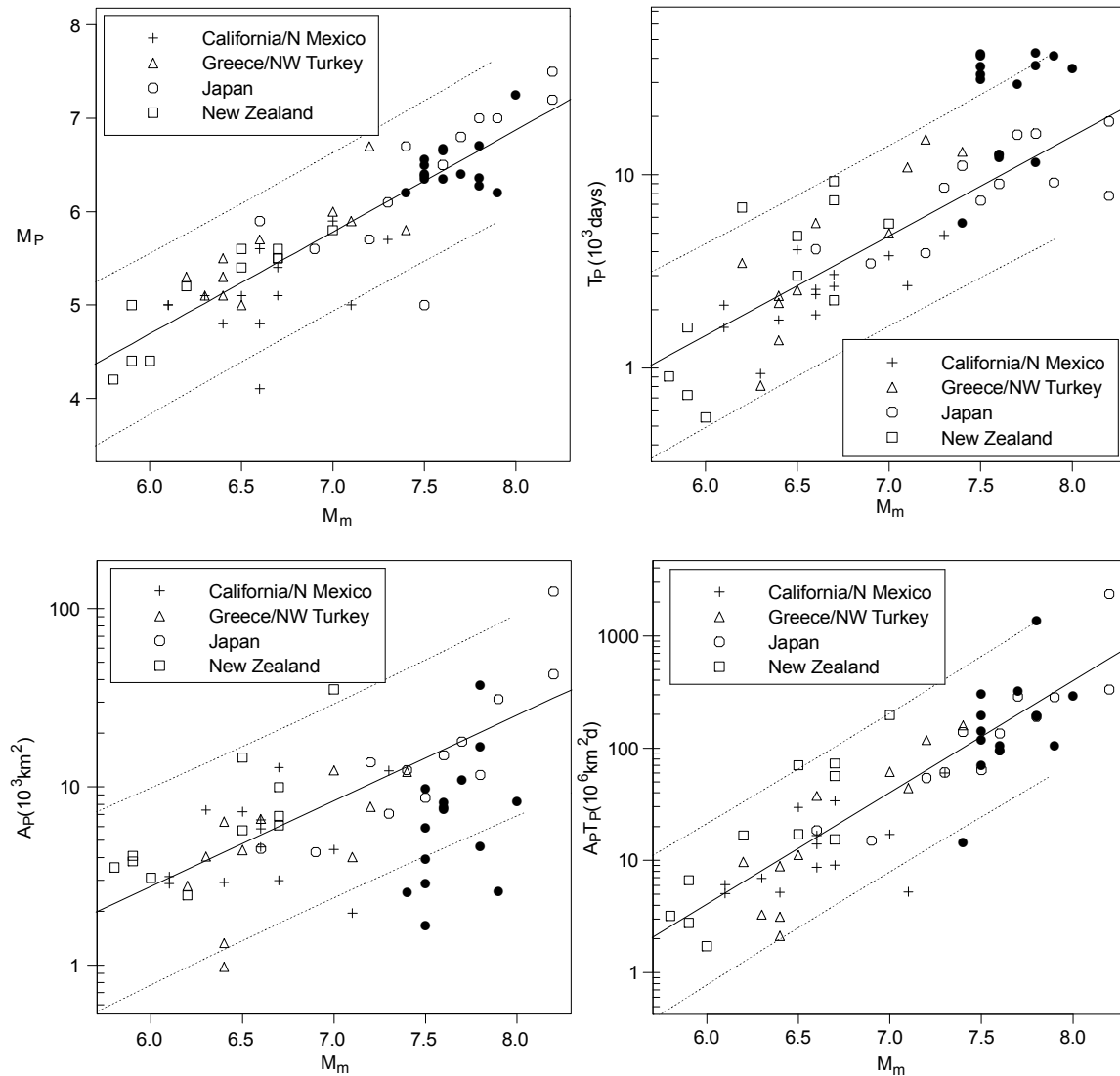


Figure 9 Precursory scale increase scaling relations between mainshock magnitude M_m and (a) precursor magnitude M_P ; (b) precursor time T_P ; (c) precursor area A_P (d) the product $A_P T_P$. Dotted lines indicate 95% tolerance limits calculated from real-world catalogues. Open symbols are used for data from real catalogues (Evison and Rhoades, 2004), and solid dots for those from synthetic catalogue derived from network B.

The correlation between $A_P T_P$ in real-world examples is noticeably higher than that between T_P and M_m and between A_P and M_m (Evison and Rhoades, 2004). The reason for this is not entirely clear. It has been noted that in regions of relatively high seismicity, such as Kanto, the precursor times tend to be shorter than in regions of relatively lower seismicity, such as

California (Rhoades, 2009), and this effect is easily understood. In the present synthetic seismicity model, the rate of seismicity could be increased, and the precursor times reduced, simply by increasing the driving force. What is not so easy to understand is why the precursory areas in regions of higher seismicity should also be smaller than those in other regions. It is intriguing that the synthetic catalogue appears to confirm this effect. However, there appears to be no mechanism in the synthetic seismicity model to affect the size of the precursory areas if the driving force were increased. Therefore, it seems most likely that the apparent confirmation of this effect by the synthetic catalogue is fortuitous.

In the synthetic seismicity model, it is possible to trace the state of each cell through time. Figure 10 shows the evolution of shear stress and strength on a single cell on the Wellington Fault in the synthetic seismicity model through five seismic cycles over a period of some 3500 years. The cell is near the hypocentres of all the large events on the fault during the period and is the initiation point for the last large event. The strength is rather consistent throughout the period. It deviates only briefly from a constant value, when the cell is involved in a rupture, because of the rapid healing assumed in the model. In contrast, there are large excursions of shear stress on the time scale of the seismic cycle. The stress drops markedly upon the occurrence of a major event and generally increases in the intervening period due to the driving force in the model, but can either increase or decrease as a result of other earthquakes. However we note that during each cycle, the shear stress increases markedly on this cell at some point of time between 50 and 250 years prior to the next large earthquake. Such a sudden increase in stress in the long-term lead-up to a large earthquake is the kind of effect which, if observed regionally over the precursory area, would be capable of triggering the precursory scale increase phenomenon. However, the lead times of the increases in Figure 10, for this single cell, do not correspond closely to the corresponding precursor times for the Ψ -phenomenon, determined from a regional analysis similar to those in Figures 1 and 8, so further analysis would be required to relate these increases directly to the precursor scale increase phenomenon.

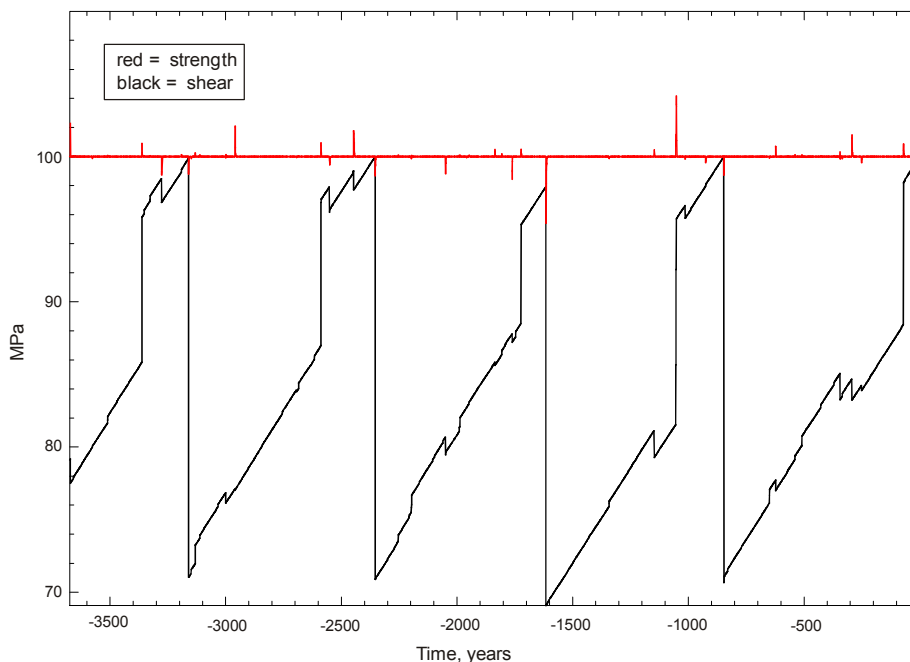


Figure 10 Shear stress (MPa, black) and strength (MPa, red) of one particular cell on the Wellington Fault through several seismic cycles. The cell is near all the hypocentres of the large events shown and is the initiation point for the last large event.

Overall, the results from both the EEPAS model and Ψ analyses indicate that the precursory scale increase is a normal feature of major earthquakes in the synthetic catalogue from network B, and that the precursor times are rather longer, and the precursory areas smaller, than those in previously studied real-world catalogues. Otherwise, the EEPAS model parameters and information score for the synthetic catalogue are similar to those for real-world catalogues. It has not been possible to analyse the smaller earthquakes in the synthetic catalogue for evidence of the precursory scale increase phenomenon, because the synthetic catalogue does not have as wide a range of magnitudes as is seen in real-world catalogues.

7.0 CONCLUSION

This study has shown that the EEPAS method and the synthetic seismicity catalogue for Network B are basically compatible in terms of the long-term precursory seismicity patterns preceding major earthquakes, lending increased credence to both. However, the synthetic catalogue for fault Network A is not compatible with EEPAS. For the moment we can only speculate why this might be. A likely explanation is that a certain degree of geometric complexity in a fault network is required for the Ψ -phenomenon to emerge. A more complete study, perhaps looking at a range of fault networks of differing complexity, would be desirable.

The precursor times are longer in the synthetic catalogue for Network B than in real catalogues, and the precursory areas smaller. Again, we can only suggest some possible reasons. The synthetic catalogue's precursor times could be reduced simply by increasing the loading rates. However, Network B was based on the real Wellington region fault network and the long-term slip rates must match the observed geologic rates, so not too much of an increase would be allowed. Another possible factor is the lack of visco-elastic relaxation in the present synthetic model. Relaxation would introduce a time dependence that is of the same order as the precursor times in the EEPAS model, and would also introduce a mechanism by which the observed inter-relations between precursor time and precursor could possibly be accounted for.

As mentioned above, the Network A synthetic catalogue has already been examined for the presence of the AMR forecasting pattern, and found wanting. Network B should now be tested for AMR in the same way.

8.0 ACKNOWLEDGEMENTS

This work was funded by the EQC Research Foundation under project number BIE 08/558. A. Christophersen and M Stirling have provided helpful reviews of the report.

9.0 REFERENCES

- Akaike, H. (1974). A new look at the statistical model identification, IEEE Trans. Automatic Control AC-19, 716-723.
- Aki, K. and P. Richards (2002), Quantitative Seismology, 2nd Edition. University Science Books, Herndon, VA, USA.

- Beeler, N., R. Simpson, A. Lockner, and S. Hickman (2000). Pore fluid pressure, apparent friction and Coulomb failure, *J. Geophys. Res.*, 105, 25,533- 25,554.
- Benites, R., Robinson, R., Webb, T. and McGinty, P. (2003). Modelling realistic ruptures on the Wellington Fault. Geological and Nuclear Sciences Client Report, 2002/85.
- Ben-Zion, Y. (1996), Stress, slip and earthquakes in models of complex single-fault systems incorporating brittle and creep deformation, *Journal of Geophysical Research*, 101, 5677-5708.
- Byerlee, J. D. (1978), Friction of rocks. *Pure and Applied Geophysics*, 116, 615-626.
- Console, R., Rhoades, D.A., Murru, M., Evison, F.F., Papadimitriou, E.E., and V.G. Karakostas, (2006). Comparative performance of time-invariant, long-range and short-range forecasting models on the earthquake catalogue of Greece, *Journal of Geophysical Research* 111, B09304, doi:10.1029/2005JB004113.
- Dieterich, J. (1994). Earthquake simulations with time-dependent nucleation and long-range interactions. In: Proceedings of the 9th joint meeting of the U.J.N.R. Panel on Earthquake Prediction Technology, Anonymous. Proceedings of the Joint Meeting of the U.J.N.R. Panel on Earthquake Prediction Technology, 9 241-268.
- Evison, F.F. (1977). The precursory earthquake swarm, *Physics of the Earth and Planetary Interiors* 15, 19-23.
- Evison, F.F. and D.A. Rhoades (2002). Precursory scale increase and long-term seismogenesis in California and northern Mexico, *Annals of Geophysics*, 45(3/4), 479-495.
- Evison, F.F. and D.A. Rhoades (2004) Demarcation and scaling of long-term seismogenesis. *Pure and applied geophysics*, 161(1): 21-45.
- Fitzenz, D. and S. Miller (2001). A forward model for earthquake generation on interacting faults including tectonics, fluids, and stress transfer, *Journal of Geophysical Research*, 106, 26,689-26,706.
- Heaton, T. (1990). Evidence for and implications of self-healing pulses of slip in earthquake rupture, *Physics of the Earth & Planetary Interiors*, 64, 1-20.
- Okada, Y. (1992). Internal deformation due to shear and tensile faults in a half-space, *Bulletin of the Seismological Society of America*, 82, 1018-1040.
- Raleigh, C. B., Healy, J. and Bredehoft, J. (1976). An experiment in earthquake control at Rangely, Colorado. *Science*, 191, 1230-1237.
- Rhoades, D.A. (2007). Application of the EEPAS model to forecasting earthquakes of moderate magnitude in southern California, *Seismological Research Letters* 78(1), 110-115.
- Rhoades, D.A. (2009). Long-range earthquake forecasting allowing for aftershocks, *Geophys. J. Int.* 178, 244-256.

- Rhoades, D.A. and F.F. Evison (2004). Long-range earthquake forecasting with every earthquake a precursor according to scale, *Pure Appl. Geophys.* 161(1), 47-71.
- Rhoades, D.A. and F.F. Evison (2005). Test of the EEPAS forecasting model on the Japan earthquake catalogue, *Pure and applied geophysics*, 162(6/7): 1271-1290.
- Rhoades, D.A. and F.F. Evison (2006). The EEPAS forecasting model and the probability of moderate-to-large earthquakes in central Japan, *Tectonophysics*, 417(1/2): 119-130.
- Rhoades, D.A. and M.C. Gerstenberger (2009). Mixture models for improved short-term earthquake forecasting, *Bull. Seismol. Soc. Amer.*, 99(2), 636-646.
- Robinson, R. (2004). Potential Earthquake Triggering in A Complex Fault Network: The Northern South Island, New Zealand, *Geophysical Journal International*, 159, 734-748.
- Robinson, R. and R. Benites (1996). Synthetic Seismicity Models for the Wellington Region, New Zealand: Implications for the Temporal Distribution of Large Events, *Journal of Geophysical Research*, 101, 27,833-27,845.
- Robinson, R. and R. Benites (2001), Upgrading a synthetic seismicity model for more realistic fault ruptures, *Geophysical Research Letters* 28, 1843-1846.
- Robinson, R., Zhou, S., Johnston, S., and Vere-Jones, D., (2005). Precursory Accelerating Seismic Moment Release (AMR) in a Synthetic Seismicity Catalog; A Preliminary Study. *Geophysical Research Letters*, 32, L07309, doi:10.1029/2005GL022576.
- Robinson, R., A. Nicol, J. Walsh and P. Villamor (2009). Features of earthquake occurrence in a complex normal fault network: Results from a synthetic seismicity model of the Taupo Rift, New Zealand. In Press: *Journal of Geophysical Research*.
- Rundle, P., J. Rundle, K. Tiampo., A. Donnellan and D. Turcotte (2006). Virtual California: fault model, frictional parameters, applications, *Pure and Applied Geophysics*, 163, 1819-1846.
- Ward, S. (2000). San Francisco Bay Area earthquake simulations: a step toward a standard physical earthquake model, *Bulletin of the Seismological Society of America*, 90, 370 - 386.
- Wesnousky, S. (2008), Displacement and Geometrical Characteristics of Earthquake Surface Ruptures: Issues and Implications for Seismic-Hazard Analysis and the Process of Earthquake Rupture, *Bulletin of the Seismological Society of America*, 98, 1609 - 1632.
- Zhou, S., Johnston, S., Robinson, R. and Vere-Jones, D., 2006. Tests of the Precursory Accelerating Moment Release (AMR) Model using a Synthetic Seismicity Model for Wellington, New Zealand. *J. Geophys. Res.*, 111, B05308, doi:10.1029/2005JB003720.



www.gns.cri.nz

Principal Location

1 Fairway Drive
Avalon
PO Box 30368
Lower Hutt
New Zealand
T +64-4-570 1444
F +64-4-570 4600

Other Locations

Dunedin Research Centre
764 Cumberland Street
Private Bag 1930
Dunedin
New Zealand
T +64-3-477 4050
F +64-3-477 5232

Wairakei Research Centre
114 Karetoto Road
Wairakei
Private Bag 2000, Taupo
New Zealand
T +64-7-374 8211
F +64-7-374 8199

National Isotope Centre
30 Gracefield Road
PO Box 31312
Lower Hutt
New Zealand
T +64-4-570 1444
F +64-4-570 4657